Applied Surface Science 258 (2012) 7059–7063

Contents lists available at SciVerse ScienceDirect

Applied Surface Science

journal homepage: www.elsevier.com/locate/apsusc

Morphology on 3D ordered macroporous metals associated to deposition depth

Wuhong Xin[a], Lili Yang[b], Jiupeng Zhao[c,*], Yao Li[a,*]

[a] Center for Composite Materials and Structure, Harbin Institute of Technology, No. 92 Xidazhi Street, Harbin 150001, PR China
[b] School of Transportation Science and Engineering, Harbin Institute of Technology, Harbin 150001, PR China
[c] School of Chemical Science and Technology, Harbin Institute of Technology, Harbin 150001, PR China

ARTICLE INFO

Article history:
Received 18 November 2011
Received in revised form 28 March 2012
Accepted 29 March 2012
Available online 4 April 2012

Keywords:
Three-dimensionally (3D) ordered macroporous materials
Morphology
FeNi
Electrodeposition

ABSTRACT

High quality three-dimensionally (3D) ordered macroporous FeNi has been fabricated using the electrodeposition method assisted by colloidal crystal templates. The architectures are composed of highly ordered close-packed spherical pores interconnected. The material of this characteristic structure has potential applications in the fields of catalysts, electrodes, and sensors. The morphology of 3D ordered macroporous metals along the (1 1 1) direction is determined by the deposition depth (film thickness). In this work, the observed surface morphology is discussed in terms of subsequently increasing film thickness. Models are set up to help with full understanding of the evolution of the morphology (the shapes of the pore mouths and pore walls).

1. Introduction

Three-dimensionally (3D) ordered macroporous materials are periodic dielectrics which are long-range ordered in three dimensions [1–5]. Materials being designed into 3D ordered macroporous architectures have become a research hotspot due to the high surface-to-volume ratio, well-defined pore dimensions and precisely controlled three-dimensional ordering [6].

For the potential applications of 3D ordered macroporous materials, a wide range of fabrication technologies have been proposed. These technologies can be simply divided into direct and indirect methods. Direct synthesis routes including multibeam interference lithography, bio-templating method, direct laser writing and direct ink writing, have been used to fabricate 3D ordered macroporous structures [4,7,3,8]. However, lithography, direct laser writing and direct ink writing methods are now facing the difficulty of high cost and time consumption, while bio-templating method has the disadvantage of small scale products limiting the practical applications. An efficient and low cost indirect approach including self-assembly of artificial opal (template) and replication of the template has been proposed and widely accepted. For the replication process, various methods such as wet chemistry techniques, chemical vapor deposition, atomic layer deposition and electrodeposition have been used to achieve the duplicated architectures [9–13].

Electrodeposition can be used to prepare well ordered, supported thin films in a remarkable short time. The deposited materials occupy just the interstices between the polystyrene (PS) spheres and the thickness of the deposit can be simply controlled by regulating the deposition time applied [14–16]. Hence we adopted electrodepositon for the fabrication of 3D ordered macroporous FeNi.

3D ordered macroporous materials obtained from high filling fraction structure, which is known as residual volume structure [17], have the potential to produce complete photonic band gap. One major difference from residual volume structure to low filling fraction structures such as skeleton structure and shell structure is the morphology variation of the product along the (1 1 1) direction as the electrodeposition is carried on. Therefore, the diameter of the pore mouths can be used to estimate the film thickness [6,18–20]. However, detailed discussion focused on the relationship between the shape of the pore mouths and the deposition depth (film thickness) has not been published. In this article, 3D ordered macroporous FeNi has been prepared by applying a constant current density of 0.03 A/cm^2, and the template was removed by toluene etching to leave 3D ordered macroporous product. The evolution of the morphology of the film was discussed and found to be associated to the deposition depth. Disordered macroporous FeNi electrodeposited is also presented to study the different diffusion rates in disordered template.

2. Experimental

2.1. Materials

Reagents used were monodisperse PS spheres, ferrous sulfate heptahydrate ($FeSO_4{\cdot}7H_2O$), nickel sulfate hexahydrate

* Corresponding authors. Tel.: +86 451 89263976; fax: +86 451 86402345.
E-mail addresses: jpzhao@hit.edu.cn (J. Zhao), liyao@hit.edu.cn (Y. Li).

0169-4332/$ – see front matter © 2012 Elsevier B.V. All rights reserved.
http://dx.doi.org/10.1016/j.apsusc.2012.03.177

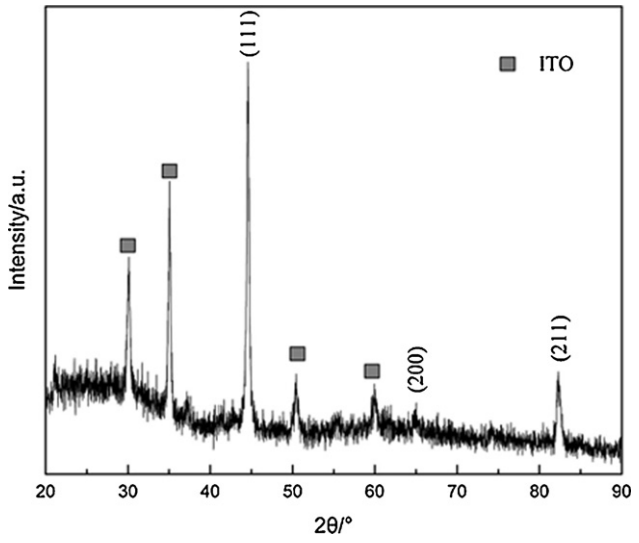

Fig. 1. X-ray diffraction pattern of 3D ordered macroporous FeNi alloy thin film electrodeposited on the ITO substrate after the removal of the template.

($NiSO_4{\cdot}6H_2O$), boric acid (H_3BO_3), sulphuric acid (H_2SO_4) and toluene (C_7H_8). All chemicals were of analytical reagent grade and were used without further purification. Water used in all experiments was purified with a resistivity greater than 18 MΩ/cm. Indium tin oxide (ITO) substrate with a sheet resistance of 15 Ω/sq was cut into 1 cm × 4 cm pieces for the self-assembly of colloidal crystals.

2.2. Preparation of 3D ordered macroporous FeNi alloy films

The monodisperse PS latex with a concentration of 0.1% was added into cylindrical vessels. Clean ITO substrates were put into the vessels at 55 ± 0.2 °C. After complete volatilization of water, the highly uniform PS colloidal microspheres were formed on the substrate surface and displayed a typical iridescent behavior due to Bragg diffraction.

The electrodeposition was carried on in a two-electrode system. The PS-coated ITO glass was used as working electrode (WE), and the plating solution (Fe^{2+} and Ni^{2+}) can reach the ITO layer through the interstitial spaces of the PS colloidal crystals. A platinum flake was used as counter electrode (CE). The electrodeposition of FeNi alloy was achieved by applying a constant current density of 0.03 A/cm^2. And the deposit was washed with water immediately after deposition to remove other chemicals. The PS template was then removed by immersing in toluene for 24 h and 3D ordered macroporous FeNi products were thus obtained.

2.3. Characterization

The morphologies of the products were characterized by a Hitachi S-4800 scanning electron microscope (SEM) with an accelerating voltage of 20 kV. The phase composition of the architectures was analyzed by using X-ray diffraction (XRD) on a Phillips X Pert diffractometer equipped with CuKα radiation in the range of $2\theta = 20–90°$.

3. Results and discussion

3.1. Characterization of 3D ordered macroporous FeNi

Fig. 1 shows the X-ray diffraction pattern of the 3D ordered macroporous FeNi thin film electrodeposited on the ITO substrate after the PS template has been removed. The peaks at $2\theta = 44.5°$, 64.9° and 82.3° can be indexed as (1 1 1), (2 0 0) and (2 1 1) reflections of the alloy, respectively. The diffraction pattern illustrates typical reflection peaks of cubic FeNi alloy (JCPDF#65-7251) and displays a (1 1 1) preferred orientation. The intensity of (2 0 0) diffraction peak is weak, indicating that the supporting film is thin. The crystalline grain size of the product estimated from the width of (1 1 1) peak at half maximum is 18 nm using the Debye–Scherrer formula. And the rest peaks at $2\theta = 30.2°$, 35.0°, 50.5° and 60.1° can be identified to (2 2 2), (4 0 0), (4 4 1) and (6 2 2) reflections of the ITO coater (JCPDF#39-1058).

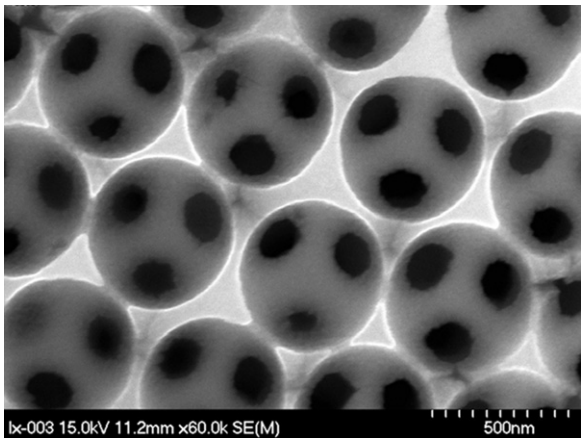

Fig. 2. High resolution image of 3D ordered macroporous FeNi alloy film deposited.

Fig. 2 shows a macroporous FeNi film electrodeposited. The three pores into the layer below are clearly visible, demonstrating the three-dimensional ordering of the architecture. According to theoretical analysis, point windows should be left around the regions where the original spheres were in contact when the deposition (infiltration) is complete. However, connections are generated for polymeric sphere during the self-assembly process thus leading to larger pore windows rather than point windows.

3.2. Morphology variation of 3D ordered macroporous metals

Fig. 3 shows the SEM image of the resulting film with a gradient thickness after the removal of the template. This image can be divided into 6 regions as the increase of the film thickness (marked by A–F). The morphology varies gradually from region A to region F. The shape of the pore mouths in region A (regions B and C) is the

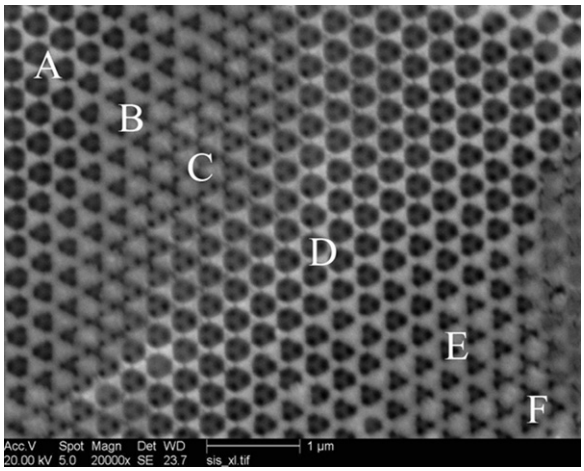

Fig. 3. The morphology of a macroporous FeNi film with a gradient thickness electrodeposited through a template assembled from 320 nm diameter spheres.

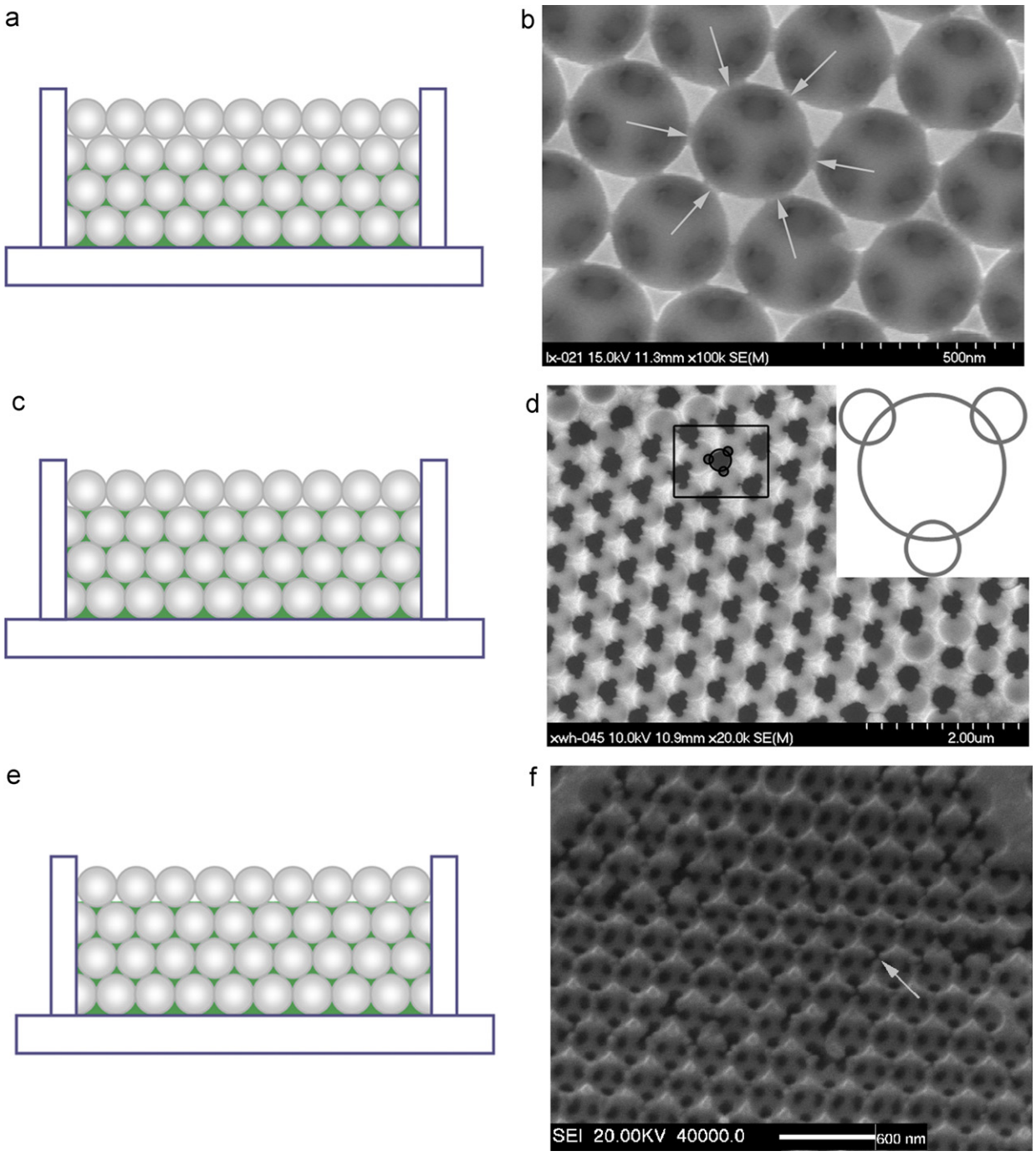

Fig. 4. Models of side view (perpendicular to (1 1 1) plane) of the inverse opals and the corresponding SEM images toward (1 1 1) plane at typical film thicknesses.

same as they exhibit in region D (regions E and F). New layers are formed in regions B and E, respectively. In order to help with full understanding of the evolution of the morphology as the increase of the deposition depth, we set up a range of models of the products with different thicknesses.

Models of the products of typical film thicknesses are summarized in Fig. 4. Fig. 4a shows the perpendicular view to (1 1 1) plane of a region where the film thickness can be expressed by

$$h = \left(1 + \frac{2\sqrt{6}}{3}(n-1)\right) r$$

where h is the thickness of the film, r is the radius of the PS spheres used as templates and n is the number of the layers. Here in this formula, $(2\sqrt{6}/3)r$ is the vertical distance from the bottom of a sphere to the bottom of another sphere assembled on the first one. Thus, it can be considered as a unit to count the depth below the layer which is partially infiltrated by the targeted materials. The corresponding SEM image toward (1 1 1) plane of the 3D ordered macroporous FeNi is illustrated in Fig. 4b. The shape of the pore mouths is circular and the pore walls are composed of six triangular depositions which are replicas of the former octahedral and tetrahedral voids of the opal structure [21]. And the octahedral and tetrahedral voids of the layer which is being infiltrated are half occupied at this deposition depth as shown [9]. In the direction parallel to (1 1 1) plane, there are six pore windows (indicated by arrows in Fig. 4b) which originate from the connections formed between neighboring spheres.

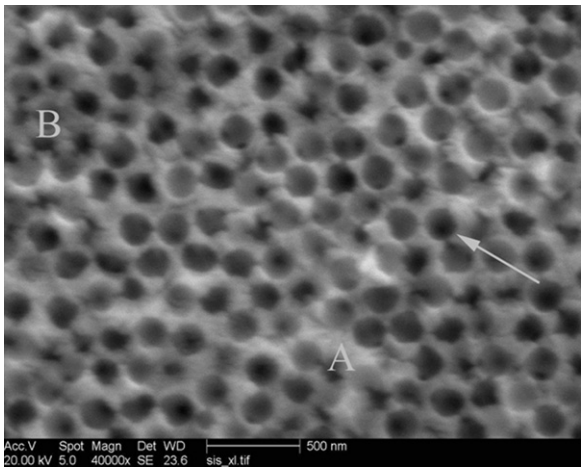

Fig. 5. The morphology of the disordered macroporous FeNi alloy electrodeposited.

The side view and the corresponding SEM image of FeNi are shown in Fig. 4c and d, and the film thickness can be estimated by

$$h = \left(1 + \frac{\sqrt{6}}{3} + \frac{2\sqrt{6}}{3}(n-1)\right) r$$

As shown in Fig. 4c, the interstices of the top PS layer are partially filled and the interstices of the layer below are not totally occupied at this deposition depth. In this formula, $(\sqrt{6}/3)r$ is the vertical distance between the center of the underlayer sphere and the surface of the infiltrated materials. The triangular pore mouths are indicative of the formation of a new layer according to the geometry of the packing of the spheres in the template [22]. The formation of the rounded triangular pore mouths is caused by the connections of the original colloidal template which cannot be occupied by the deposit. Moreover, the pore mouths are actually round in shape as shown in the inset of Fig. 4d [18].

The side view and the corresponding SEM image of FeNi product are shown in Fig. 4e and f, the film thickness of which can be represented as

$$h = \left(2 + \frac{2\sqrt{6}}{3}(n-1)\right) r$$

The interstices of the underlayer spheres are fully filled at this deposition depth. The small pore (marked by an arrow) corresponds to the top position of the original polymeric sphere of the layer below which is the one of the vertices of the octahedral void. Similar small pores have been observed for other porous materials [18]. The existence of the small pores can be assigned to different diffusion rates of the reactant in these regions within the template. Normally, larger void spaces lead to faster diffusion rate thus faster deposition rate [23]. And as the deposition is going on, these regions become filled in by the metal.

3.3. Morphology of macroporous metals obtained from disordered template

Fig. 5 shows the morphology of the disordered macroporous FeNi electrodeposited. The final alloy is interconnected through the pore windows which originate from the connections (as indicated by an arrow). It has been reported that the quality of the colloidal crystal templates plays an important role in the morphologies of the materials obtained [23]. Poorly ordered templates give channels that allow different diffusion rates and result in uneven deposits. The whiter and darker positions (marked by A and B respectively) in this image represent the higher and lower positions of the deposit.

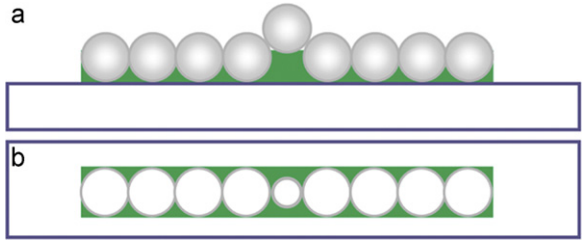

Fig. 6. Schematic illustration of (a) side view and (b) top view of the colloidal template assembled with one sphere arranged at higher position than other spheres of the same layer.

Meanwhile, the pore mouths are of different diameters due to the disordered template. As illustrated in Fig. 6, PS sphere which is arranged at higher position than other spheres of the same layer occupies smaller space, leading to smaller pore mouth. This is the case of ordered template with point defect. For disordered template, pore mouths of different sizes are left. Moreover, it is noted that some pore mouths are not circular in shape which can be attributed to the uneven film surface.

4. Conclusion

In this work, 3D ordered macroporous FeNi films have been fabricated through electrodeposition in a two-electrode system under the guidance of colloidal templates. The evolution of the surface morphology as the increase of the deposition depth has been systematic studied. The results indicate that the variation of the shape of the pore mouths is repeatable during the deposition. When the film thickness is $(1 + (2\sqrt{6}/3)(n-1))r$, the shape of the pore mouths is circular and the pore walls are composed of six triangular depositions. When the film thickness is $(1 + (\sqrt{6}/3) + (2\sqrt{6}/3)(n-1))r$, the pore mouths are of rounded triangular in shape and a new layer is formed. And when the film thickness is $(2 + (2\sqrt{6}/3)(n-1))r$, the triangular pore walls are formed. Replicas obtained from disordered template are also discussed. The noncircular pore mouths and the uneven film are mainly caused by different diffusion rates in channels of the disordered template.

Acknowledgements

We thank the National Natural Science Foundation of China (nos. 51010005, 90916020, 51174063), the Program for New Century Excellent Talents in University (NCET-08-0168), the Fundamental Research Funds for the Central Universities (HIT.ICRST.2010001) and Sino-German joint project (GZ550) for financial support.

References

[1] A. Imhof, D.J. Pine, Nature 389 (1997) 948–951.
[2] M. Miyake, Y.C. Chen, P.V. Braun, P. Wiltzius, Advanced Materials 21 (2009) 3012–3015.
[3] J.W. Galusha, L.R. Richey, M.R. Jorgensen, J.S. Gardner, M.H. Bartl, Journal of Materials Chemistry 20 (2010) 1277–1284.
[4] W.H. Xin, J.P. Zhao, Y.B. Ding, Y. Li, Applied Surface Science 257 (2011) 10725–10728.
[5] M. Deubel, G. von Freymann, M. Wegener, S. Pereira, K. Busch, C.M. Soukoulis, Nature Materials 3 (2004) 444–447.
[6] Y.W. Hao, F.Q. Zhu, C.L. Chien, P.C. Searson, Journal of the Electrochemical Society 152 (2007) D65–D69.
[7] M. Miyake, Y.-C. Chen, P.V. Braun, P. Wiltzius, Advanced Materials 21 (2009) 3012–3015.
[8] G.M. Gratson, M.J. Xu, J.A. Lewis, Nature 428 (2004) 386.
[9] L. Xu, L.D. Tung, L. Spinu, A.A. Zakhidov, R.H. Baughman, J.B. Wiley, Advanced Materials 15 (2003) 1562.
[10] A. Blanco, C. López, R. Mayoral, H. Míguez, F. Meseguer, A. Mifsud, J. Herrero, Applied Physics Letters 73 (1998) 1781.
[11] R.W.J. Scott, S.M. Yang, G. Chabanis, N. Coombs, D.E. Williams, G.A. Ozin, Advanced Materials 13 (2001) 1468.

[12] J.S. King, E. Graugnard, C.J. Summers, Advanced Materials 17 (2005) 1010.
[13] P.N. Bartlett, M.A. Ghanem, I.S.E. Hallag, P. de Groot, A. Zhukov, Journal of Materials Chemistry 13 (2003) 2596.
[14] P.V. Braun, P. Wiltzius, Nature 402 (1999) 603.
[15] P.V. Braun, P. Wiltzius, Advanced Materials 13 (2001) 482.
[16] H. Mguez, E. Chomski, F. Garci-Santamari, M. Ibisate, S. John, C. Loez, F. Meseguer, J.P. Mondia, G.A. Ozin, O. Toader, H.M. van Driel, Advanced Materials 13 (2001) 1634.
[17] M. Sadakane, C. Takahashi, N. Kato, H. Ogihara, Y. Nodasaka, Y. Doi, Y. Hinatsu, W. Ueda, Bulletin of the Chemical Society of Japan 80 (2007) 677–685.
[18] P.N. Bartlett, J.J. Baumberg, P.R. Birkin, M.A. Ghanem, M.C. Netti, Chemistry of Materials 14 (2002) 2199–2208.
[19] P.N. Bartlett, T. Dunford, M.A. Ghanem, Journal of Materials Chemistry 12 (2002) 3130–3135.
[20] P.N. Bartlett, J.J. Baumberg, S. Coyle, M.E. Abdelsalam, Faraday Discussions 125 (2004) 117–132.
[21] D. Hung, Z. Liu, N. Shah, Y.W. Hao, P.C. Searson, Journal of Physical Chemistry C 111 (2007) 3308–3313.
[22] X. Li, Y. Jiang, Z.W. Shi, Z. Xu, Chemistry of Materials 19 (2007) 5424–5430.
[23] P.N. Bartlett, P.R. Birkin, M.A. Ghanem, Chemical Communications (2000) 1671–1672.